


## Ionization of atoms and molecules using 200-keV protons and 5.5-MeV/u bare C ions: Energy-dependent collision dynamics

Madhusree Roy Chowdhury,<sup>1,2</sup> A. Mandal,<sup>1</sup> A. Bhogale,<sup>1</sup> H. Bansal,<sup>1</sup> C. Bagdia,<sup>1</sup> S. Bhattacharjee,<sup>1</sup> J. M. Monti <sup>3</sup>,  
R. D. Rivarola,<sup>3</sup> and Lokesh C. Tribedi<sup>1,\*</sup>

<sup>1</sup>Tata Institute of Fundamental Research, Homi Bhabha Road, Colaba, Mumbai 400005, India

<sup>2</sup>M. S. University of Baroda, Vadodra 390001, India

<sup>3</sup>Instituto de Fisica Rosario, CONICET, Universidad Nacional de Rosario, 2000 Rosario, Argentina



(Received 17 March 2020; revised 16 June 2020; accepted 1 July 2020; published 28 July 2020)

Using electron spectroscopy technique, we measure the absolute double-differential cross sections (DDCSs) of electrons emitted in collisions of 200-keV protons on He, CH<sub>4</sub>, and O<sub>2</sub> and 5.5-MeV/u bare C ions colliding on O<sub>2</sub>. The emitted electrons are measured in the energy range from 1 to 400 eV for He and CH<sub>4</sub> targets and up to 600 eV for O<sub>2</sub> to include the *K*-*LL* Auger line of oxygen. The electrons are detected over different emission angles varying from 20° in the extreme forward direction to 160° in the backward direction. The single-differential cross section (SDCS) and total cross section are deduced from the measured DDCSs spectra for all the targets. The DDCS and SDCS are compared with the state-of-the-art continuum distorted wave–eikonal initial state (CDW-EIS) theoretical model. The CDW-EIS model provides excellent agreement with the oxygen data at MeV energy, whereas the deviation in the case of keV energy is substantial, in spite of having nearly the same perturbation strength. The forward-backward angular asymmetry shows a saturation effect in the case of keV energy protons but no such signature is observed for the high-energy collision. A systematic analysis reveals that the asymmetry at low electron energy is sensitive to the associated atomic or molecular structure and is in close agreement with the theory.

DOI: [10.1103/PhysRevA.102.012819](https://doi.org/10.1103/PhysRevA.102.012819)

### I. INTRODUCTION

The ionization of atomic and molecular targets by the impact of charged particles has been a subject of study over the decades and still draws attention in different fields such as astrophysics, plasma physics (particularly for the modeling of the low-temperature plasmas), and radiation therapy for cancer treatment [1–3]. In this work we focus on the study of single ionization of three different atomic and molecular targets, such as He, CH<sub>4</sub>, and O<sub>2</sub> in collisions with keV energy protons. To understand how the ionization dynamics changes with the variation in the velocity  $v_p$  and charge state  $q_p$  of the projectile, we provide a comparative study for the ionization of the O<sub>2</sub> molecule using keV energy protons and MeV energy C<sup>6+</sup> ions. These two projectiles were chosen such that, although the  $q_p$  and  $v_p$  are quite different, their perturbation strengths  $q_p/v_p$  are nearly the same, i.e., 0.35 for the 200-keV/u protons and 0.40 for the 5.5-MeV/u C<sup>6+</sup> ions.

The collision of protons on He is one of the simplest and a benchmark system for testing the efficacy of the theoretical models on ion-atom collisions. Helium is also one of the most abundant elements found in the universe. The protons and  $\alpha$  particles are present abundantly in the solar wind, which is a highly ionized magnetized plasma. The CH<sub>4</sub> is one of the important molecules which is present in the interstellar medium, in the circumstellar environment, on the surface of

Titan, and also on the surfaces of several icy bodies of the solar system [4,5]. The methane-containing surfaces are exposed to the energetic protons and other ions from the cosmic rays leading to the ionization and fragmentation of the molecules. A better understanding of the ionization cross sections of these molecules is thus essential for modeling the various planetary atmospheres and for other astrophysical applications.

Although the molecular targets, such as CH<sub>4</sub> and O<sub>2</sub>, are more complicated compared to He, they act as benchmark or reference targets for studying the ionization of large biomolecules [6], which have gained immense importance for hadron therapy (for a recent review see [1,2]). The methane also serves as a reference system for studying the large hydrocarbon molecules such as the polycyclic aromatic hydrocarbon molecules in connection with an application in astrochemistry. Therefore, these small molecular targets serve as a bridge between the small atoms and large molecules and provide a stringent test of the theoretical models before they are applied for the larger molecules. Apart from these applications, ionization studies of diatomic molecules such as O<sub>2</sub>, H<sub>2</sub>, and N<sub>2</sub> have also gained renewed interest due to the observation of the Young-type interference effect in the electron-emission spectrum due to spatial coherence, a fundamental quantum-mechanical interest [7–12]. The study of such atoms and molecules is also crucial towards the development of a comprehensive scaling law for ionization (see, for example, the work by Montenegro *et al.* [13]).

Over the past few decades, several studies have been carried out on the double-differential cross sections (DDCSs)

\*lokesh@tifr.res.in; ltribedi@gmail.com

of electrons emitted from a helium atom using the protons and highly charged ions having energies from a few keV to several MeV [14–30]. Different studies on the ionization, fragmentation, and charge-transfer processes [31–34] have also been carried out for CH<sub>4</sub> and O<sub>2</sub> targets. However, not many measurements of the DDCS of electron emission from CH<sub>4</sub> and O<sub>2</sub> exist in the literature [35–41]. Studies on the total ionization cross sections are the most common, although the DDCS measurements provide a much better understanding of the collision dynamics.

In the present experiment, besides the high-energy collision ( $v_p \sim 15$  a.u.), we also measure the electron emission at a lower velocity ( $v_p \sim 2.8$  a.u.), which is closer to the intermediate-velocity regime where along with ionization, electron capture and transfer ionization channels are also effective. In most of the earlier work on DDCS measurements of electron emission from He by protons [15–17], the measured data were compared with the first Born approximation, a one-center model, which is well known to work only for projectiles with high energy and does not deal with postcollisional effects. In contrast, the continuum distorted wave–eikonal initial state (CDW-EIS) model is well known to be effective in the intermediate- to high-energy regime of the projectile. This model assumes the ionized electron to be influenced by the long-range Coulomb field of both the target and the projectile, thus explaining the two-center effect accurately. The present series of experiments using both the He atom and simple molecules along with an elaborate comparison with the CDW-EIS model provides valuable inputs towards the understanding of the collision dynamics in the low- and high-velocity regimes.

We report the energy and angular distributions of the DDCS of the electrons emitted from He, CH<sub>4</sub>, and O<sub>2</sub> in collisions with 200-keV/u protons along with the same for O<sub>2</sub> with 5.5-MeV/u bare C ions. The forward-backward angular asymmetry  $\alpha(k)$ , which reflects well on the two-center effect and also the characteristics of the target, is deduced for all three targets. In our experiments with 200-keV H<sup>+</sup> ions, since the projectile velocity is almost comparable to the velocity of the valence electrons in the target,  $\alpha(k)$  is an even more important quantity to study.

## II. EXPERIMENTAL TECHNIQUES

A brief description of the experimental apparatus is given here. The 200-keV protons (velocity  $v_p = 2.83$  a.u.) were obtained from the electron cyclotron resonance–based ion accelerator facility at TIFR, Mumbai [42,43]. This is a 14.5-GHz machine with a maximum extraction voltage of 30 kV. The electron cyclotron resonance (ECR) plasma ion source along with an electrostatic lens, Faraday cup, and analyzing magnet is mounted on a high-voltage deck which can be raised up to 400 kV. This low-energy accelerator is suitable for providing low-velocity highly charged ions. There are four beamlines and a switching magnet is used to steer the beam in the desired beamline. Each beamline is equipped with electrostatic quadrupole triplet lenses and X-Y deflectors for focusing and steering the ion beam. A pair of four jawed slits is also used to cut the beam and control the beam divergence. A differential pumping arrangement is connected at the end

of the beamline, which is followed by the scattering chamber. An extended aperture, 2 mm in diameter and 30 mm long, is placed at the end of the beamline and another aperture of 4 mm diameter is placed just at the entrance of the scattering chamber for further beam collimation. The beamline pressure is maintained at about  $5 \times 10^{-9}$  mbar and the scattering chamber is maintained at a base pressure of  $10^{-8}$  mbar. It is necessary to maintain a high vacuum in the beamline to reduce the probability of charge neutralization of the projectile ions. In the case of He and CH<sub>4</sub>, the scattering chamber is flooded with the target gases at an absolute pressure of 0.1 and 0.05 mTorr, respectively, which is measured using a capacitance manometer (MKS Baratron). In the case of O<sub>2</sub>, the experiments are performed both under flooded chamber conditions and by using an effusive jet source; in both cases similar results are obtained. In the case of the effusive jet source, the experiment is performed in a crossed-beam arrangement. Two sets of  $\mu$  metal sheets are attached to the inner walls of the scattering chamber to reduce the Earth’s magnetic field to about 10 mG near the interaction region. The ejected electrons are energy analyzed using the hemispherical electrostatic energy analyzer and are further detected by the channel electron multiplier (CEM). A preacceleration voltage  $V_c$  of 6 V is applied at the entrance and exit slits of the spectrometer to increase the collection efficiency of the low-energy electrons. The resolution of the analyzer is 6% of the electron energy. The front of the CEM is biased to +100 V, which ensures a uniform collection efficiency of the detector in the electron energy range measured. The number of projectile ions is obtained by measuring the ion beam current on the Faraday cup. The DDCSs are measured in both the presence and absence of the target gas for all the angles, although the background counts in the absence of the target gas are very low. The ejected electrons from He and CH<sub>4</sub> are measured between 1 and 400 eV and for O<sub>2</sub> from 1 to 600 eV. The measurements for all three targets impacted by 200-keV protons are performed for 11 different angles from 20° to 160°. The total absolute error in the present series of experiments varies from 15% to 19%, which includes contributions from gas pressure fluctuations, counting statistics, efficiency of the detector, resolution of the spectrometer, and the solid-angle path-length integral. The statistical error varies from  $\sim 1\%$  in the case of the forward angles to  $\sim 8\%$  for the higher energies in the extreme backward angles, where the cross section falls by order of magnitude. However, below 10 eV some more systematic error cannot be ruled out, which is difficult to estimate.

A similar kind of setup is used to perform the measurements for the O<sub>2</sub> target using a MeV energy ion beam. The 66-MeV C<sup>5+</sup> ions ( $v_p = 14.9$  a.u.) were obtained from the 14-MV BARC-TIFR Pelletron Accelerator Facility at TIFR, Mumbai. The energy and charge state analyzed C<sup>5+</sup> ions are passed through a poststripper carbon foil arrangement to obtain the bare ions. The C<sup>6+</sup> ions are selected using a switching magnet and directed to the desired beamline. The rest of the experimental techniques and the arrangement comprising the scattering chamber, differential pumping station, and electron analyzer are similar to those in the case of measurements with 200-keV H<sup>+</sup> ions. The experiment is performed under flooded chamber conditions at a static absolute pressure of

0.15 mTorr and the DDCS spectra for electrons emitted from O<sub>2</sub> are measured for 12 different angles, namely, 20°, 30°, 45°, 60°, 75°, 80°, 90°, 105°, 120°, 135°, 150°, and 160°.

### III. THEORETICAL DESCRIPTION

An independent-particle approximation is employed to describe the single-ionization reaction. This means that only one electron from each one of the atomic or molecular orbitals is considered to be ionized, whereas all the other target electrons (the passive electrons) are considered to remain frozen in their initial orbitals. The ionization process is described within the prior form of the CDW-EIS formalism within the straight-line version of the impact parameter approximation used for the calculations [44,45]. The scattering amplitude as a function of the impact parameter in the prior version within the CDW-EIS approximation can be written as [46]

$$A_{if}^-(\rho) = -i \int_{-\infty}^{+\infty} dt \left\langle \chi_f^- \left| \left[ \left( H_{el} - i \frac{\partial}{\partial t} \right) \chi_i^+ \right] \right. \right\rangle, \quad (1)$$

where  $H_{el}$  is the one-active-electron Hamiltonian and  $\chi_f^-$  and  $\chi_i^+$  are the final and initial channel distorted wave functions, respectively, given by

$$\chi_i^+ = \varphi_i(\mathbf{x}) \exp(-i\varepsilon_i t) \exp[-i\nu \ln(v s + \mathbf{v} \cdot \mathbf{s})], \quad (2)$$

$$\begin{aligned} \chi_f^- = & \varphi_f(\mathbf{x}) \exp(-i\varepsilon_f t) N^*(\lambda) {}_1F_1[-i\lambda; 1; -i(kx - \mathbf{k} \cdot \mathbf{x})] \\ & \times N^*(\xi) {}_1F_1[-i\xi; 1; -i(ps - \mathbf{p} \cdot \mathbf{s})], \end{aligned} \quad (3)$$

with  $\mathbf{x}$  ( $\mathbf{s}$ ) the active-electron coordinate in a target-fixed (projectile-fixed) reference frame. In (2)  $\varphi_i$  represents the active-electron initial bound state with  $\varepsilon_i$  its initial binding energy and  $\nu = Z_p/v$  with  $Z_p$  the projectile charge and  $v$  the collision velocity. In (3)  $\varphi_f$  is a free-electron plane wave with momentum  $\mathbf{k}$ ,  $\varepsilon_f = \frac{1}{2}k^2$ ,  $\xi = Z_p/p$ ,  $\mathbf{p} = \mathbf{k} - \mathbf{v}$ , and  $\lambda = \tilde{Z}_T/k$  with  $\tilde{Z}_T$  and the effective target nuclear charge describing the interaction of the active electron with an effective residual-target Coulomb potential. Also  ${}_1F_1$  is the hypergeometric function and  $N(a) = \exp(\pi a/2)\Gamma(1 - ia)$  its normalization factor (with  $\Gamma$  the Euler Gamma function). The initial bound state of the He target was considered within a Roothaan-Hartree-Fock (RHF) representation [47]. In the case of the O<sub>2</sub> target, the molecule was approximated simply by two independent oxygen atoms also described by RHF functions [47]. The CH<sub>4</sub> molecule was represented by a linear combination of atomic orbitals (LCAO) within a complete neglect of differential overlap (CNDO) approximation (see [37,48]).

In all cases the residual-target continuum state effective charge is taken as  $\tilde{Z}_T = n_i \sqrt{-2\varepsilon_i}$ . In the He and O cases,  $n_i$  is the principal quantum number of the atomic orbital and  $\varepsilon_i$  its ionization energy. In the CH<sub>4</sub> case,  $\varepsilon_i$  is now the molecular orbital ionization energy and  $n_i$  the principal quantum number of the corresponding atomic orbital in the LCAO.

This model was applied with very good success, first for mono-electronic atomic targets [49], and since then it has been continuously upgraded (see, for example, the review by Fainstein *et al.* [22]). The model was then extended to multi-electronic atomic targets [44] by including numerical wave functions. The CDW-EIS model has been further improved in order to apply it to small [46,50] and larger biological [51]

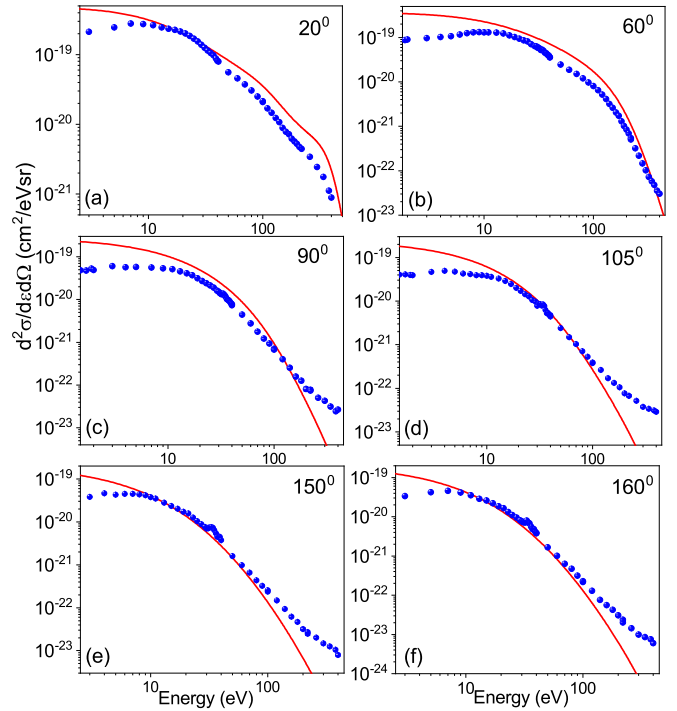


FIG. 1. Absolute electron DDCS for He as a function of emission energies for different forward and backward angles. The solid line in each panel shows the CDW-EIS model calculation.

molecules. Such a developed model has been successfully applied to compare experimental data for methane [38], adenine [3,6], and other large molecules.

## IV. RESULTS AND DISCUSSION

### A. Energy distribution of the electron DDCS

#### 1. 200-keV proton impact

The absolute DDCSs of the electrons emitted from He for six different electron-emission angles are displayed in Fig. 1. The small peak seen in the backward angles at around 35 eV corresponds to the autoionization process following a double excitation. In the case of forward angles, due to the large Coulomb ionization contribution, the autoionization peak is not observed. The CDW-EIS model provides qualitatively overall good agreement with the data for all the forward angles. In the case of the backward angles, the model matches well with data points up to about 70 eV, beyond which it underestimates the data for the rest of the spectra. For the lowest electron energies (i.e., between 1 and 10 eV), the experimental uncertainties are large, as there could be insufficient collection of electrons due to any stray fields causing additional systematic errors. This may explain only a part of the deviation between the theory and experiment at these low energies.

Figure 2 displays the energy distribution curves for CH<sub>4</sub> at different forward and backward emission angles. The DDCS falls by several orders of magnitude with an increase in ejected-electron energy for a fixed emission angle. The sharp peak observed in the backward angles at about 240 eV corresponds to the *K*-*LL* Auger electron emission from carbon

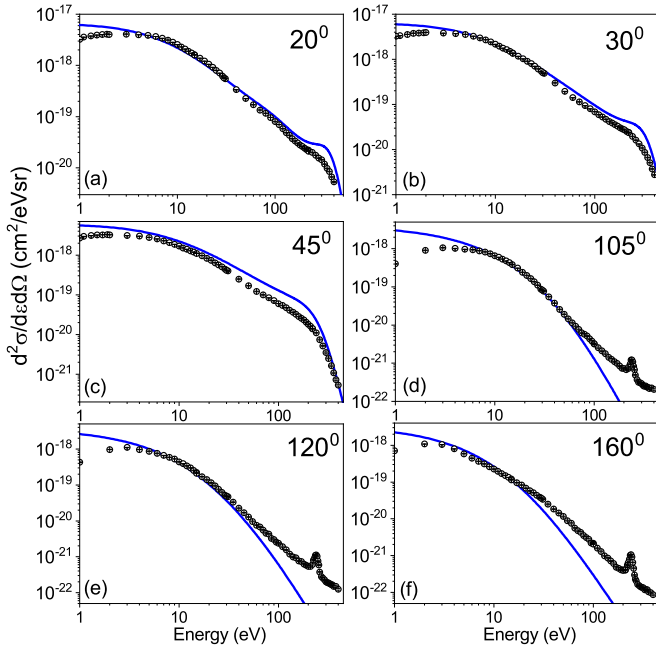


FIG. 2. Same as Fig. 1 but for 200-keV  $H^+$  ions impacting on  $CH_4$ .

which occurs when a vacancy exists in the inner shell. Overall very good agreement is observed between the theoretical model and experimental data for the forward angles, whereas in the backward angles one observes good agreement up to about 50 eV, beyond which the theory shows a discrepancy with the measured data. A small humplike structure can be seen in the forward angles around 250–300 eV at  $30^\circ$  both experimentally and theoretically. This hump is due to the binary nature of the collision or head-on collision between the projectile and the target electron. The position of the binary encounter (BE) peak is given by  $E = 4 \cos^2 \theta m_e (\frac{E_p}{M_p})$ , where  $M_p$  is the mass of the projectile having energy  $E_p$  and  $m_e$  is the mass of the electron emitted with energy  $E$  at an emission angle  $\theta$ . For the present experiment of 200-keV  $H^+$  ions, at  $30^\circ$ , the peak should be observed at 300 eV, whereas for an emission angle of  $45^\circ$ , it should be observed at 200 eV. If the target electron is initially at rest, then one would expect a prominent peak; however, an electron bound to an atom or molecule has an initial momentum distribution which superimposes on the peak. In the present case, the projectile velocity is 2.83 a.u., which is almost comparable to the orbital velocity of the electrons (1 a.u.) in the outermost shell of  $CH_4$  and hence the initial velocity distribution of the target electrons completely smears out the binary peak over the entire range of emission energies.

Similarly, Fig. 3 shows the electron-emission DDCS spectra for  $O_2$  when bombarded with 200-keV  $H^+$  ions; the solid curves correspond to twice the theoretical calculations for atomic oxygen. For the present collision system, a large discrepancy is observed between the measured data and the calculations for all the emission angles, although any obvious reason for the same is not known. The  $K$ - $LL$  Auger electron-emission peak is seen at around 480 eV for all the backward

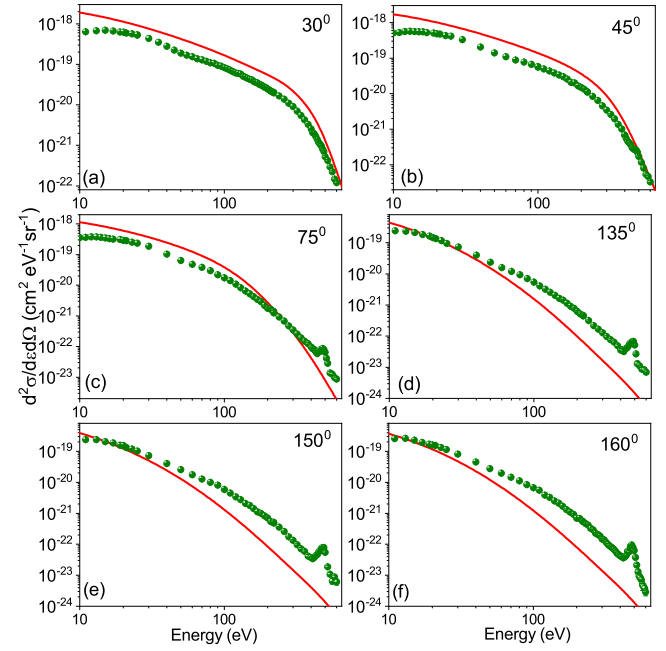


FIG. 3. Absolute electron DDCS for six different emission angles for collision of 200-keV protons on  $O_2$ . Solid lines represent the CDW-EIS calculations for atomic oxygen multiplied by 2.

angles, whereas for forward angles it becomes invisible due to the large continuum cross sections.

## 2. 66-MeV bare C ion impact

The energy distribution of the electrons ejected due to collision of  $C^{6+}$  ions with  $O_2$  is shown in Fig. 4. The low-energy part of the spectrum is dominated by the soft col-

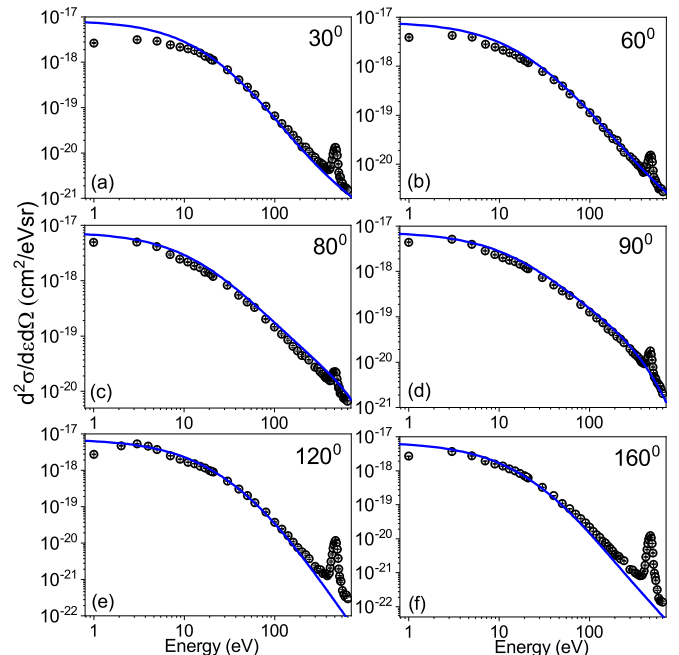


FIG. 4. Same as Fig. 3 but for the collision system of 66-MeV  $C^{6+}$  ions impacting on  $O_2$ .



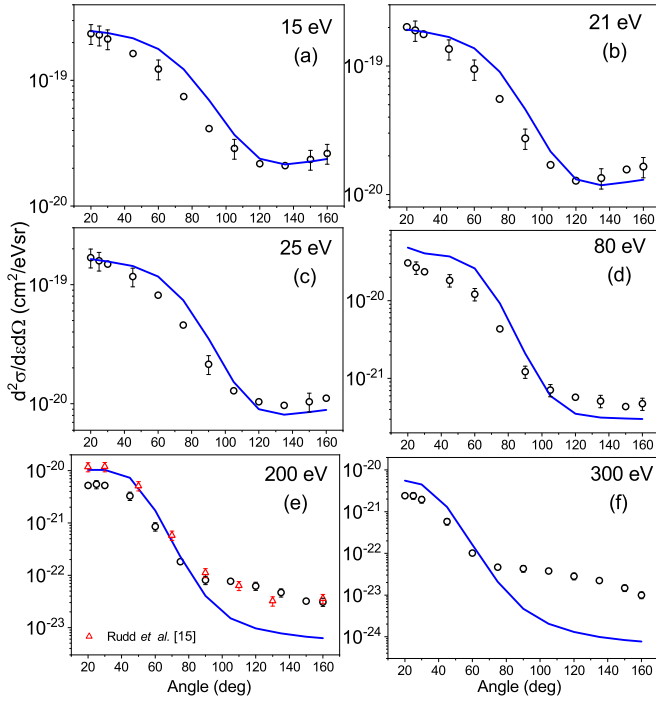


FIG. 5. DDCS of ejected electrons from He as a function of emission angle for different emission energies (black open circles). The solid curves show the CDW-EIS model calculations.

lision or glancing collision mechanism where the electrons are emitted with a large impact parameter. In the case of highly charged ions like  $C^{6+}$ , the two-center effect plays an important role which generates the intermediate part of the spectrum. Moving further ahead in the spectrum, one can see the  $K$ - $LL$  Auger peak at  $\sim 480$  eV for oxygen. For the present projectile, since  $v_p$  is much larger compared to the orbital velocity of the target electrons, the BE peak will be present at a much higher emission energy in the case of the extreme forward angles. The CDW-EIS model for twice the atomic oxygen provides excellent agreement with the experimental data points for all the angles and over the entire energy range under investigation. Only in the case of extreme backward angles, at the higher-energy side of the spectrum, the theory underestimates the data.

### B. Angular distribution of the electron DDCS

Figure 5 shows the angular distribution in the case of the He target for different electron-emission energies. A large angular asymmetry is observed between the extreme forward and extreme backward angles even in the case of low emission energies such as 15 eV. The asymmetry increases even further with an increase in emission energy. This large angular asymmetry between the forward and backward angles may be explained by the two-center collision mechanism, as mentioned in the preceding section. In the case of the atomic target He, excellent agreement is observed between the measured data and the theoretical model for low-emission energies such as 15, 21, and 25 eV. With an increase in emission energy, although qualitative agreement is observed between the theoretical curves and measured quantities, quantitatively it is seen

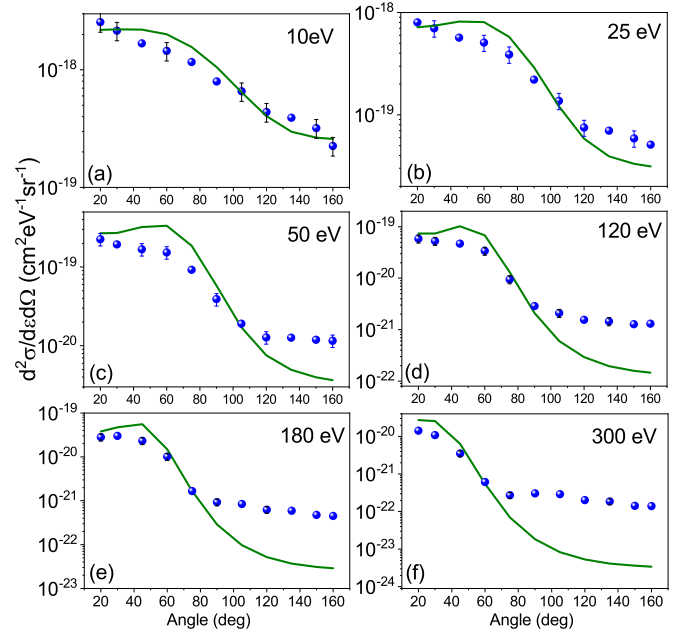


FIG. 6. Angular distribution of the electron DDCS for  $CH_4$  at fixed electron-emission energies along with the theoretical calculations.

that theory slightly overestimates the data for forward angles and underestimates the data points for the backward angles. For higher emission energies, the departure of the theory from the experimental measurements increases even further for the backward angles. The experimental electron DDCS for He reported by Rudd *et al.* [15] is shown in Fig. 5(e) by red triangles. These points match well with the present data for the backward angles but are a factor of 2 times higher for the extreme forward angles. In Figs. 6 and 7, similar results are observed between theoretical curves and experimental data for

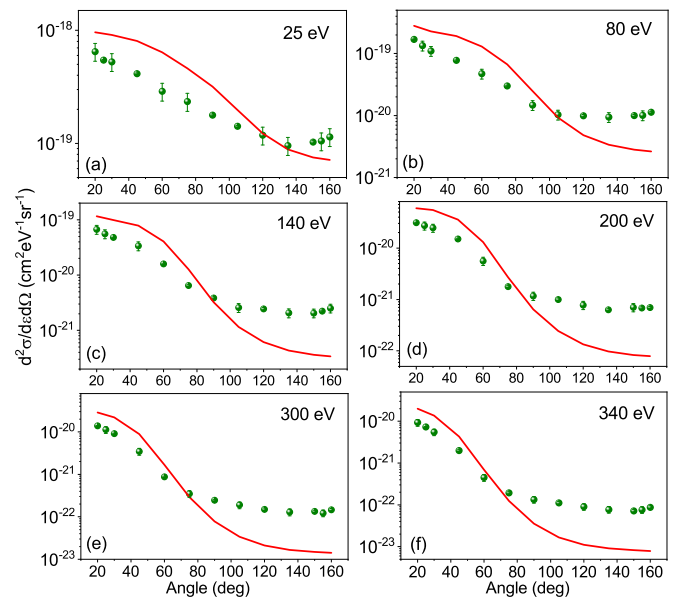


FIG. 7. Angular distribution of  $e^-$  DDCS from  $O_2$  in collisions with 200-keV protons along with CDW-EIS calculations.

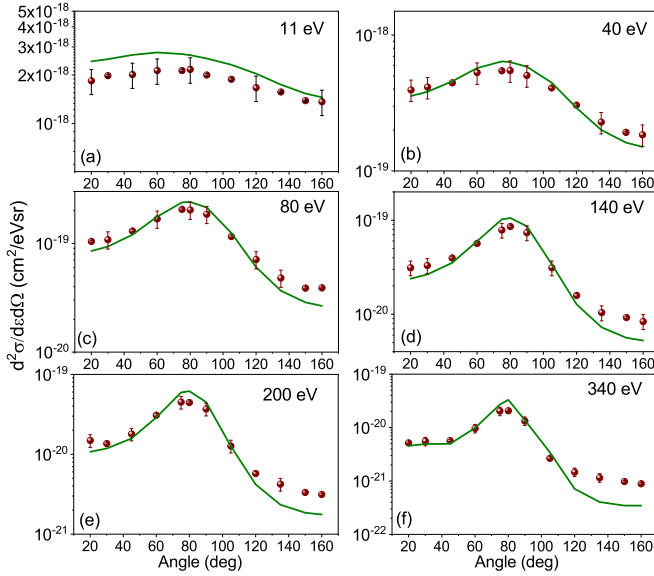


FIG. 8. Same as Fig. 7 but for 66-MeV  $C^{6+}$  ions colliding with  $O_2$ .

both targets,  $CH_4$  and  $O_2$  in collisions with 200-keV  $H^+$  ions. In all the cases, the CDW-EIS model agrees qualitatively with data, but quantitatively shows maximum discrepancies in the backward angles for higher emission energies. In Figs. 5–7, the total absolute error bars are shown for some of the points. From the angular distribution plots, the CDW-EIS model is seen to work well particularly for forward angles.

In Fig. 8 we present the DDCS of electrons as a function of emission angle for the 66-MeV  $C^{6+}$  ion impact on the  $O_2$  target gas. The angular distribution plots shown in the six panels for different electron energies reveal a completely different trend from that observed in Fig. 7. In the case of 11 eV [Fig. 8(a)], we observe an almost flat distribution over the entire angular spread. This is due to the dominance of the soft-collision mechanism, indicating isotropic ionization over all angles. For higher electron energies, a peak is seen around  $80^\circ$  which gets sharper with an increase in electron emission-energy. This peak is due to the binary-collision mechanism. Except for the lowest energies, the forward angles have higher cross sections compared to the backward angles, which is due to the two-center effect. For 80 eV, the DDCS for extreme forward angles is 2.7 times higher than for the extreme backward angles. This factor increases further with higher emission energies and in the case of 340 eV it is about 6 times higher than for backward angles, indicating a drastic fall of cross sections in the case of backward angles. The CDW-EIS model shows overall good agreement with the measured data, except for the higher energies for backward angles, where it underestimates the data.

### C. Forward-backward angular asymmetry

Following the prescription of Fainstein *et al.* [52], we define the forward-backward angular asymmetry parameter  $\alpha(k)$  as

$$\alpha(k, \theta) = \frac{\sigma(k, \theta) - \sigma(k, \pi - \theta)}{\sigma(k, \theta) + \sigma(k, \pi - \theta)}, \quad (4)$$

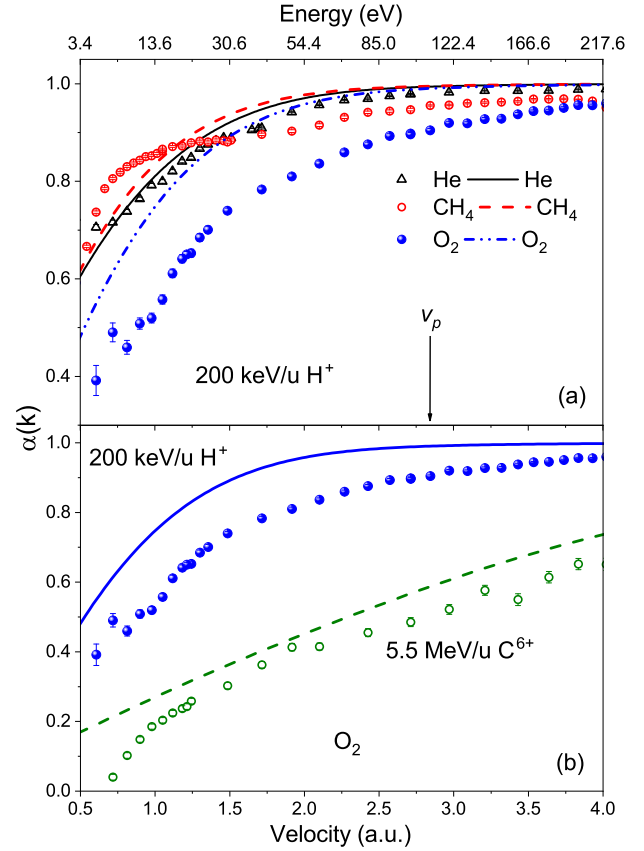


FIG. 9. Asymmetry parameter  $\alpha(k)$  for (a) three different targets bombarded by the same projectile and (b)  $O_2$  impacted by 200-keV protons and 66-MeV  $C^{6+}$  ions. All lines indicate CDW-EIS model predictions.

where the electron energy  $\epsilon_k = \frac{k^2}{2}$  in a.u.,  $\theta$  is a low forward angle, and  $k$  denotes the ejected-electron velocity. Since the angular distribution varies slowly near 0 and  $\pi$ , we use the measured DDCS at  $20^\circ$  to calculate the approximate value of the asymmetry parameter, i.e.,  $\alpha(k)$  for all four collision systems under investigation (shown in Fig. 9). For He and  $CH_4$ , a large asymmetry is observed which increases monotonically from 0.7 to  $\sim 1.0$ , showing a tendency to saturate beyond  $k = 2.75$  a.u., as shown in Fig. 9(a). Theory predicts similar behavior, showing overall good agreement for He. However, experimentally  $CH_4$  shows a slightly different shape compared to that for He as well as that predicted by the CDW-EIS calculation. For 200-keV protons colliding on  $O_2$ , the  $\alpha(k)$  increases monotonically from 0.4 to  $\sim 1.0$  and saturates beyond 2.75 a.u. One may note that although the shapes of the angular distributions at the lower-energy (keV) and higher-energy (MeV) collisions are vastly different, the asymmetry parameter reveals similar kind of distributions as a function of  $k$ . This gives us a way to compare the data in a widely different projectile energy range. It is obvious from Fig. 9(b) that the  $\alpha(k)$  values for 200-keV/u protons are much larger than that for the collisions with high energy, i.e., 5.5-MeV/u  $C^{6+}$  ions. This may be explained by the fact that the two-center effect and postcollisional interactions are much stronger for 200-keV protons than for the higher-energy

TABLE I. Total ionization cross section in units of Mb for the four collision systems.

Target	Projectile	$q_p/v_p$	TCS		Ratio
			Expt. ( $\pm 18\%$ )	CDW-EIS	
He	200-keV/u $H^+$ ions	0.35	31.5	50.7	1.6
CH <sub>4</sub>	200-keV/u $H^+$ ions	0.35	252	346	1.4
O <sub>2</sub>	200-keV/u $H^+$ ions	0.35	148	337	2.3
O <sub>2</sub>	5.5-MeV/u $C^{6+}$ ions	0.40	708	809	1.14

projectiles, although the perturbation strengths, i.e.,  $q_p/v_p$ , for both projectiles are almost same. Thus, the asymmetry parameter cannot be characterized uniquely by the perturbation strength; rather it depends independently on the actual value of the  $q_p$  and the  $v_p$ . It can be seen from Fig. 9(a) that for lower electron energies  $\alpha(k)$  is sensitive to the atomic or molecular structure of the target and has the lowest value for the O<sub>2</sub>, followed by the He and CH<sub>4</sub> targets. For these low-energy electrons, the impact parameters are expected to be large and the projectile interacts with the whole atom or molecule. In such cases the momentum transfer is small and thereby the ejected electrons are sensitive to the structure of the atom or the molecule. With an increase in the electron velocity, the  $\alpha(k)$  tend to merge together, since for these electron velocities the impact parameter is quite small and hence the projectile interacts mostly with individual atoms in the molecule. Another feature that is observed for all three targets is the saturation effect. This effect is seen to occur when the electron velocity is close to or above the velocity of the projectile. In the case of 66-MeV bare C ions, with the projectile velocity being much higher than the highest value of  $k$  measured, the  $\alpha(k)$  values keep on increasing with the increase in the electron velocity. Therefore, the angular asymmetry is another or complementary way to look into the information about collision dynamics and its dependence on molecular species.

#### D. Single-differential cross section

The measured DDCS spectra can be used to obtain the single-differential cross section (SDCS) by integrating the DDCS over one of the variables, either the measured emission energies or the emission angles. Figure 10(a) shows the SDCS as a function of emission angles for all three targets He, CH<sub>4</sub>, and O<sub>2</sub> along with the CDW-EIS calculations. The SDCSs obtained experimentally and theoretically for methane have been multiplied by a factor of 4 (shown in the figure). For all three targets, the SDCSs have been obtained by integrating the data from 5 to 400 eV. The CDW-EIS prediction matches well with the experimentally obtained SDCS for the He atom, although it slightly overestimates the data. In the case of CH<sub>4</sub>, the theory shows qualitative agreement with excellent matching around 100°–120°. Contrary to the above two targets, for O<sub>2</sub>, a wide deviation is observed between experimental and theoretical SDCSs over almost the entire angular region. Figure 10(b) displays the SDCS for the MeV energy bare C ions impacting on O<sub>2</sub>. Here also the integration has been performed between 5 and 400 eV. The distribution is

reproduced very well by the theoretical model, with excellent agreement for the backward angles.

Integrating the SDCS further over the emission angles, we get the total ionization cross section (TCS) of the collision system both experimentally and theoretically. The TCS values provided in Table I have been deduced by integrating over the electron energies from 5 to 400 eV and over the emission angles between 20° and 160°. The theoretical to experimental TCS ratios provide the best agreement for MeV energy highly charged ion projectile, whereas deviations (by a factor of 1.4–2.3) exist for 200-keV protons, with the maximum difference occurring in the case of O<sub>2</sub>. From this study it may be inferred that although  $q_p/v_p$  was nearly the same for both energies, the difference between the data and the model is not the same; rather a larger deviation is seen at the lower energy.

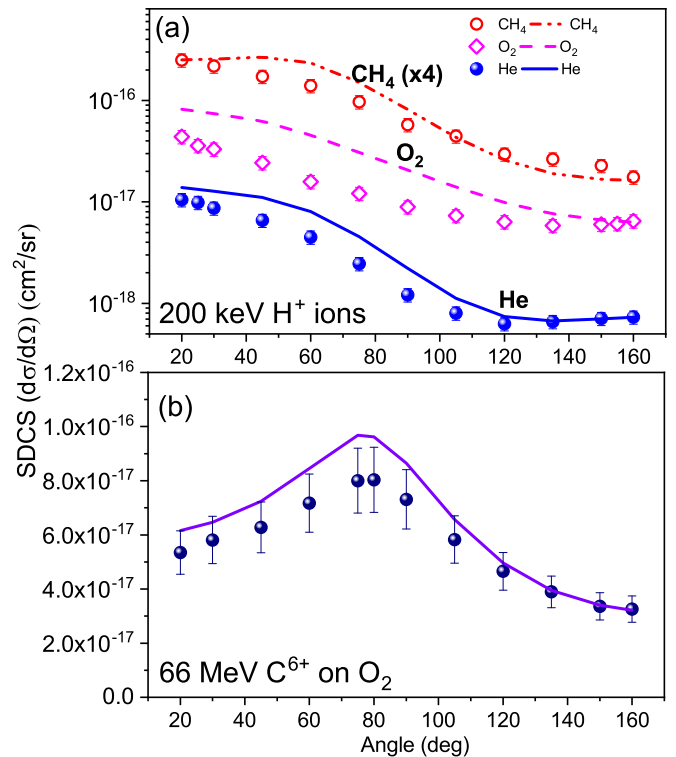


FIG. 10. SDCS as a function of emission angles for (a) all three targets in collisions with 200-keV protons along with CDW-EIS calculations (solid and dashed lines) [the data for CH<sub>4</sub> (and theory) are multiplied by 4] and (b) 66-MeV  $C^{6+}$  ions impacting on O<sub>2</sub>.

## V. CONCLUSION

We have measured the absolute DDCS of the electrons emitted from an atomic target He and two molecular targets CH<sub>4</sub> and O<sub>2</sub> when ionized by 200-keV/u protons. Double-differential cross-section measurements have also been carried out for O<sub>2</sub> in collisions with 5.5-MeV/u bare C ions. These two projectiles were chosen such that the perturbation strengths for both projectiles were nearly the same. In the case of 5.5-MeV/u bare C ions, the CDW-EIS calculations for oxygen show excellent agreement with the measured data for all the angles. For 200-keV protons, the model provides reasonably good agreement for He and CH<sub>4</sub>, but overestimates the DDCS for O<sub>2</sub> in the case of all angles. The angular distribution shows a distinctly different character for the two different projectiles. In the case of lower-energy collisions the forward-backward asymmetry parameter has a much higher value compared to that for high-energy C ions, in spite of almost the same perturbation strength. This implies that the perturbation strength  $q_p/v_p$  alone cannot characterize completely the asymmetry and two-center effect. For 200-keV protons,  $\alpha(k)$  showed a saturation effect (irrespective

of the target species) for electron velocity greater than the velocity of the projectile. The single-differential distributions were also derived. The CDW-EIS model provides the best agreement for the MeV energy collisions, whereas deviations (by a factor of 1.4–2.3) exist for the 200-keV protons with the maximum difference occurring in the case of O<sub>2</sub>, in spite of having the same perturbation strength for all the collisions. Further systematic investigations are required to check the efficacy of perturbation strength in characterizing the collision dynamics.

## ACKNOWLEDGMENTS

We would like to thank N. Mhatre, K. V. Thulasiram, W. A. Fernandes, and D. Pathare for their help during the operation of the ECR ion accelerator. We are also grateful to the staff at the BARC-TIFR Pelletron Accelerator Facility. One of the authors (M.R.C) would like to acknowledge financial assistance from Council of Scientific and Industrial Research (CSIR), India.

- 
- [1] L. C. Tribedi, in *State-of-the-Art Reviews on Energetic Ion-Atom and Ion-Molecule Collisions*, edited by D. Belkić, I. Bray, and A. Kadyrov (World Scientific, Singapore, 2019), Vol. 2, Chap. 3, pp. 59–98.
- [2] F. Aumayr, K. Ueda, E. Sokell, S. Schippers, H. Sadeghpour, F. Merkt, T. F. Gallagher, F. B. Dunning, P. Scheier, O. Echt *et al.*, *J. Phys. B* **52**, 171003 (2019).
- [3] Y. Iriki, Y. Kikuchi, M. Imai, and A. Itoh, *Phys. Rev. A* **84**, 052719 (2011).
- [4] R. V. Yelle, J. Cui, and I. C. F. Müller-Wodarg, *J. Geophys. Res.: Planet.* **113**, E10003 (2008).
- [5] A. G. G. M. Tielens, The molecular universe, *Rev. Mod. Phys.* **85**, 1021 (2013).
- [6] S. Bhattacharjee, C. Bagdia, M. R. Chowdhury, A. Mandal, J. M. Monti, R. D. Rivarola, and L. C. Tribedi, *Phys. Rev. A* **100**, 012703 (2019).
- [7] S. Nandi, A. N. Agnihotri, S. Kasthurirangan, A. Kumar, C. A. Tachino, R. D. Rivarola, F. Martín, and L. C. Tribedi, *Phys. Rev. A* **85**, 062705 (2012).
- [8] M. Winkworth, P. Fainstein, M. Galassi, J. Baran, B. Dassanayake, S. Das, A. Kayani, and J. Tanis, *Nucl. Instrum. Methods Phys. Res. Sect. B* **267**, 373 (2009).
- [9] M. Roy Chowdhury and L. C. Tribedi, *J. Phys. B* **50**, 155201 (2017).
- [10] M. Ilchen, L. Glaser, F. Scholz, P. Walter, S. Deinert, A. Rothkirch, J. Seltmann, J. Viefhaus, P. Declava, B. Langer, A. Knie, A. Ehresmann, O. M. Al-Dossary, M. Braune, G. Hartmann, A. Meissner, L. C. Tribedi, M. AlKhaldi, and U. Becker, *Phys. Rev. Lett.* **112**, 023001 (2014).
- [11] D. Misra, U. Kadhane, Y. P. Singh, L. C. Tribedi, P. D. Fainstein, and P. Richard, *Phys. Rev. Lett.* **92**, 153201 (2004).
- [12] D. Misra, A. Kelkar, U. Kadhane, A. Kumar, L. C. Tribedi, and P. D. Fainstein, *Phys. Rev. A* **74**, 060701(R) (2006).
- [13] E. C. Montenegro, G. M. Sigaud, and R. D. DuBois, *Phys. Rev. A* **87**, 012706 (2013).
- [14] M. E. Rudd and T. Jorgensen, *Phys. Rev.* **131**, 666 (1963).
- [15] M. E. Rudd, C. A. Sautter, and C. L. Bailey, *Phys. Rev.* **151**, 20 (1966).
- [16] M. E. Rudd and D. H. Madison, *Phys. Rev. A* **14**, 128 (1976).
- [17] D. H. Madison, *Phys. Rev. A* **8**, 2449 (1973).
- [18] M. E. Rudd, R. D. DuBois, L. H. Toburen, C. A. Ratcliffe, and T. V. Goffe, *Phys. Rev. A* **28**, 3244 (1983).
- [19] A. Salin, *J. Phys. B* **5**, 979 (1972).
- [20] A. Salin, *J. Phys. B* **22**, 3901 (1989).
- [21] D. K. Gibson and I. D. Reid, *J. Phys. B* **19**, 3265 (1986).
- [22] P. D. Fainstein, V. H. Ponce, and R. D. Rivarola, *J. Phys. B* **24**, 3091 (1991).
- [23] J. Berakdar, J. Briggs, and H. Klar, *Z. Phys. D* **24**, 351364 (1992).
- [24] S. T. Manson, L. H. Toburen, D. H. Madison, and N. Stolterfoht, *Phys. Rev. A* **12**, 60 (1975).
- [25] N. Stolterfoht, H. Platten, G. Schiwietz, D. Schneider, L. Gulyás, P. D. Fainstein, and A. Salin, *Phys. Rev. A* **52**, 3796 (1995).
- [26] J. H. Miller, L. H. Toburen, and S. T. Manson, *Phys. Rev. A* **27**, 1337 (1983).
- [27] J. O. P. Pedersen, P. Hvelplund, A. G. Petersen, and P. D. Fainstein, *J. Phys. B* **24**, 4001 (1991).
- [28] R. D. DuBois, L. H. Toburen, and M. E. Rudd, *Phys. Rev. A* **29**, 70 (1984).
- [29] J. M. Monti, O. A. Fojón, J. Hanssen, and R. D. Rivarola, *J. Phys. B* **42**, 195201 (2009).
- [30] L. C. Tribedi, P. Richard, L. Gulyás, and M. E. Rudd, *Phys. Rev. A* **63**, 062724 (2001).
- [31] I. Ben-Itzhak, K. D. Carnes, D. T. Johnson, P. J. Norris, and O. L. Weaver, *Phys. Rev. A* **49**, 881 (1994).
- [32] A. Salehzadeh and T. Kirchner, *Eur. Phys. J. D* **71**, 66 (2017).



- [33] M. U. Bug, E. Gargioni, H. Nettelbeck, W. Y. Baek, G. Hilgers, A. B. Rosenfeld, and H. Rabus, *Phys. Rev. E* **88**, 043308 (2013).
- [34] E. J. Angelin and R. Hippler, *J. Phys. B* **47**, 225208 (2014).
- [35] W. E. Wilson and L. H. Toburen, *Phys. Rev. A* **11**, 1303 (1975).
- [36] D. J. Lynch, L. H. Toburen, and W. E. Wilson, *J. Chem. Phys.* **64**, 2616 (1976).
- [37] C. A. Tachino, J. M. Monti, O. A. Fojón, C. Champion, and R. D. Rivarola, *J. Phys.: Conf. Ser.* **583**, 012020 (2015).
- [38] L. Gulyás, I. Tóth, and L. Nagy, *J. Phys. B* **46**, 075201 (2013).
- [39] W.-Q. Cheng, M. E. Rudd, and Y.-Y. Hsu, *Phys. Rev. A* **40**, 3599 (1989).
- [40] J. B. Crooks and M. E. Rudd, *Phys. Rev. A* **3**, 1628 (1971).
- [41] B. Hamre, J. P. Hansen, and L. Kocbach, *J. Phys. B* **32**, L127 (1999).
- [42] A. N. Agnihotri, A. H. Kelkar, S. Kasthurirangan, K. V. Thulasiram, C. A. Desai, W. A. Fernandez, and L. C. Tribedi, *Phys. Scr.* **T144**, 014038 (2011).
- [43] A. Mandal and L. Tribedi, *Nucl. Instrum. Methods Phys. Res. Sect. B* **440**, 19 (2019).
- [44] P. D. Fainstein, V. H. Ponce, and R. D. Rivarola, *J. Phys. B* **21**, 287 (1988).
- [45] S. E. Corchs, R. D. Rivarola, and J. H. McGuire, *Phys. Rev. A* **47**, 3937 (1993).
- [46] J. M. Monti, O. A. Fojón, J. Hanssen, and R. D. Rivarola, *J. Phys. B* **43**, 205203 (2010).
- [47] E. Clementi and C. Roetti, *At. Data Nucl. Data Tables* **14**, 177 (1974).
- [48] M. A. Quinto, P. R. Montenegro, J. M. Monti, O. A. Fojón, and R. D. Rivarola, *J. Phys. B* **51**, 165201 (2018).
- [49] D. S. F. Crothers and J. F. McCann, *J. Phys. B* **16**, 3229 (1983).
- [50] C. A. Tachino, J. M. Monti, O. A. Fojón, C. Champion, and R. D. Rivarola, *J. Phys. B* **47**, 035203 (2014).
- [51] M. E. Galassi, C. Champion, P. F. Weck, R. D. Rivarola, O. Fojón, and J. Hanssen, *Phys. Med. Biol.* **57**, 2081 (2012).
- [52] P. D. Fainstein, L. Gulyás, F. Martín, and A. Salin, *Phys. Rev. A* **53**, 3243 (1996).